THE JOURNAL OF PHYSICAL CHEMISTRY A

Subscriber access provided by UNIV OF LOUISIANA

A: Environmental, Combustion, and Atmospheric Chemistry; Aerosol Processes, Geochemistry, and Astrochemistry

Molecular Dynamics of Combustion Reactions in Supercritical Carbon Dioxide. Part 5: Computational Study of Ethane Dissociation and Recombination Reactions C2H6 # CH3 + CH3

Chun-Hung Wang, Artëm E. Masunov, Sergey Valer'evich Panteleev, Tim C. Allison, Sungho Chung, Chansun Lim, Yuin Jin, and Subith S Vasu

J. Phys. Chem. A, **Just Accepted Manuscript** • DOI: 10.1021/acs.jpca.9b02302 • Publication Date (Web): 29 Apr 2019

ACS Publications

is published by the American Chemical Society. 1155 Sixteenth Street N.W., Washington, DC 20036

Molecular Dynamics of Combustion Reactions in Supercritical Carbon Dioxide. Part 5: Computational Study of Ethane Dissociation and Recombination Reactions $C_2H_6 \rightleftharpoons CH_3 + CH_3$

Chun-Hung Wang,[1] Sergey V. Panteleev,[2] Artëm E. Masunov,*[1,3,4,5] Timothy C. Allison,[6] Sungho Chang,[7] Chansun Lim,[8] Yuin Jin,[8] and Subith S. Vasu*[9]

[1]*NanoScienece Technology Center, University of Central Florida, 12424 Research Parkway, Orlando, FL 32826, USA*
[2]*N. I. Lobachevsky State University of Nizhny Novgorod, Gagarin Av. 23, Nizhny Novgorod 603950, Russia*
[3]*Department of Chemistry, University of Central Florida, 4111 Libra Dr., Orlando, FL 32816, USA*
[4]*South Ural State University, Lenin pr. 76, Chelyabinsk 454080, Russia*
[5]*National Research Nuclear University MEPhI, Kashirskoye shosse 31, Moscow, 115409, Russia*
[6]*Southwest Research Institute, San Antonio, TX 78238, USA*
[7]*KEPCO Research Institute, Daejeon, Korea*
[8]*Hanwha Power Systems, Seongnam, Gyeonggi, Korea*
[9]*Center for Advanced Turbomachinery and Energy Research (CATER), Mechanical and Aerospace Engineering, University of Central Florida, Orlando, FL 32816, USA*

Abstract. Fossil fuel oxy-combustion is an emergent technology where habitual nitrogen diluent is replaced by high-pressure supercritical CO_2 (sCO_2), which increases the efficiency of energy conversion. In this study, the chemical kinetics of the combustion reaction $C_2H_6 \rightleftharpoons CH_3 + CH_3$ in sCO_2 environment is predicted at 30-1000 atm and 1000-2000 K. We adopt multiscale approach, where reactive complex is treated quantum mechanically in rigid rotor/harmonic oscillator approximation, while environment effects at different densities are taken into account by potential of mean force, produced with classical molecular dynamics (MD). Here we used Boxed MD, where enhanced sampling of infrequent events of barrier crossing is accomplished without application of bias potential. Multi-state empirical valence bond model is applied to describe free radical formation accurately at the cost of classical force field. Predicted rates at low densities agree well with the literature data. Rate constants at 300 atm is $2.41\times10^{14}\ T^{-0.20}$ exp(-77.03 kcal/mol/RT) 1/s for ethane dissociation and $8.44\times10^{-19}\ T^{1.42}$ exp(19.89 kcal/mol/RT) cm^3/molecule/s for methyl-methyl recombination.

Introduction

Carbon capture and sequestration is the important issue in fossil fuel power generation. Oxy-fuel combustion is the technology of purifying oxygen and diluting it with CO_2 prior to combustion. It simplifies the capture and storage for CO_2. The large thermal expansion coefficient of supercritical CO_2 used in oxy-fuel cycles determines increased efficiency of combustion energy conversion.[1-3] In addition, the nitrogen removal by air separation unit reduces the generation of pollutants such as NO_x. Hydrocarbon fuels, such as natural gas are the most abundant and widely used in turbine engines. Traditionally, engine is operated by converting fossil fuel energy into mechanical power and generating carbon dioxide and water. Such process wastes heat and requires large amount of water for cooling. The newly designed Allam power cycle[4-7] has the advantage of capturing the emitted CO_2 without external CO_2 capture equipment. The key feature of this cycle is that combustor is contained in high-pressure turbine. The optimized operating pressure for direct-fired supercritical CO_2 (sCO_2) combustion chamber can reach 300 atm and the percentage of CO_2 dilution is above 95% by mass.[8] Such environment provides the possibility of generating heat in sCO_2 environment (that has critical temperature of 304 K and critical pressure of 72.9 atm).

This study is a part of joined computational and experimental effort toward development of kinetic mechanism for oxy-combustion processes, valid in sCO_2 conditions. In our previous studies, we have modeled equation-of-state parameters,[9] reduced combustion mechanism,[10] and analyzed counterflow diffusion flame[11] in sCO_2 environment. We also predicted the catalytic effects of CO_2 molecule on potential energy surfaces of several reactions by quantum chemical methods,[12-17] and used molecular dynamics methods to optimize force field parameters to describe transcritical phenomena in H_2O/CO_2 mixtures,[18] and predict rate constants of some combustion reactions in sCO_2 environment.[19-21]

Ethane dissociation and its reverse reaction (methyl radical recombination) are important reactions in oxy-fuel combustion and are the main focus of this work:

$$C_2H_6 \rightarrow CH_3 + CH_3 \quad \text{(R1)}$$

$$CH_3 + CH_3 \rightarrow C_2H_6 \quad \text{(R1r)}$$

In C_1/C_2 hydrocarbon oxidation reaction, methyl radical recombination leads to ethane in pressure-dependent combustion reaction.[22] The significance of a reaction at particular operating condition can be evaluated by the sensitivity of the reaction.[23-24] Figure 1 shows the top ten normalized CO sensitive reactions in sCO_2 environment[8-9] and they are estimated by simulating an adiabatic constant pressure reactor at 300 bar by sensitivity analysis in CHEMKIN-Pro[25] and Aramco 2.0[26] mechanism. From this analysis, it is evident that R1r is an important reaction for methane combustion. Furthermore, the magnitude of chemical time scale is in the same order of flow time scale for highly CO_2 diluted methane combustion.[11] Therefore, to improve the accuracy of the mechanism predictions, it is critical to extend this mechanism to high pressures of CO_2. Reactions R1 and R1r were studied extensively by several groups. Yao *et al.* overviewed a series of large barrierless combustion reactions of hydrocarbon fuels and reviewed the most recent studies of R1 and R1r with both experiment and theory.[27] The experimental evaluation of rate constant k at high pressures are rare. Experimental measurements of k_1 (by shock tube)[28-34] and k_{1r} (by shock tube[28, 35-38] or laser photolysis[39-42]) were presented at the temperature range higher than 1,000 K and pressure range from 0.6 Torr up to 100 bar. Theoretically, quantum calculation combined with transition state theory (TST)[43-45] were used to evaluate k in high-pressure limit. CASPT2 predicts activation energy for R1 to be 96.28 kcal/mol,[46] close to experimental values 96.6-97.0 kcal/mol.[47-48] Ge *et al.* applied MP2 level of theory for geometry optimization and coupled cluster calculation for accurate single-point energy evaluation in a series of reactions, including R1 and R1r in the gas phase.[49] Other theoretical methods were applied to study R1 (such as B3LYP,[50] CASPT2,[46, 51

and RRKM[36] methods) and R1r rates (such as MRCI,[39] M06-L,[52] EOM-SF-CCSD,[53] Master equation,[54-55] RRKM,[56] and Monte Carlo[48, 57] methods).

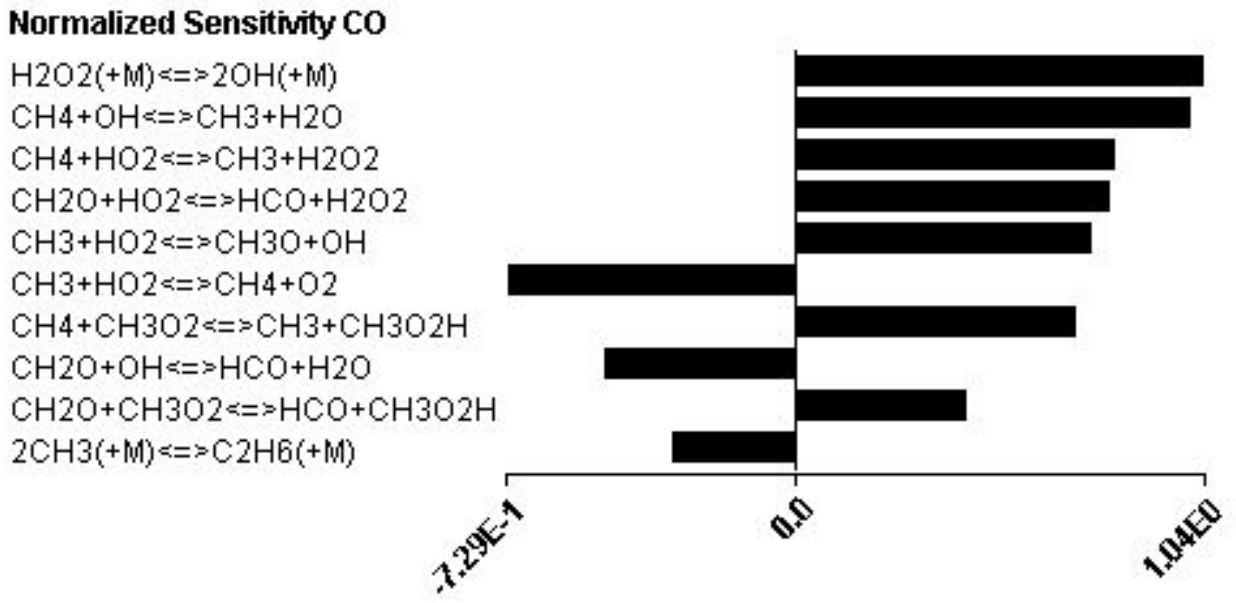

Figure 1. Normalized CO sensitivity. The initial moles of CH_4, O_2, and CO_2 are 1.0, 2.0, and 16.39, respectively.

Unlike reaction rates in the gas phase (at low density), theoretical methods for rate prediction in supercritical fluids are less developed. Akiya *et al.* have studied hydrogen peroxide dissociation ($H_2O_2 \rightarrow HO + HO$) in supercritical H_2O environment[58] and argued it can be described by equilibrium solvation effect. They proposed to combine both quantum mechanical and classical molecular dynamics methods. The potential energy surface (PES) is generated in gas phase and the reaction mechanism is assumed to be identical in the gas phase and solvent phase. The equilibrium solvation effect is quantified in terms of potential of mean force (PMF) with two contributions:

$$W(r) = \Delta E_{gas}(r) + \Delta A_{sol}(r) \quad (1)$$

where r represents the reaction coordinate, W the PMF, ΔE_{gas} is the gas-phase reaction energy, and ΔA_{sol} is the change of Helmholtz free energy in the presence of solvent. The PMF corresponds to the free energy for fixed separation O-O bond distances between the reacting molecule H_2O_2 and the equilibrated distribution of solvent H_2O molecules. The rate constant k can be obtained from Eyring-Polanyi equation from conventional TST that adequately describes the reaction:

$$k_s = \kappa\left(\frac{k_B T}{h}\right)\exp\left(-\frac{W(r^{\ddagger})}{RT}\right) \quad (2)$$

where κ is the transmission coefficient, k_B the Boltzmann constant, h the Planck constant, and $r^{\ddagger}$ is the value of the reaction coordinate at the transition state. The κ describes the probability of overcoming a potential barrier (passing through the transition state) and is assumed to be unity in TST since possible solvent-induced back scattering is not considered in this case.

Here we propose to estimate activation free energy by two components:

$$\Delta G^{\ddagger}(r) = \Delta G_{gas}(r) + \Delta\Delta G_{sol}(r) \quad (3)$$

where $\Delta G^{\ddagger}$ is the activation free energy in solution, ΔG_{gas} the gas-phase free energy change, and $\Delta\Delta G_{sol}$ the solvent free energy change. Therefore, the rate constant is modified to:

$$k = \kappa\left(\frac{k_B T}{h}\right)\exp\left(-\frac{\Delta G^{\ddagger}}{RT}\right) \quad (4)$$

PMF includes both direct (from the reactant) and indirect (from the surrounding solvent) contributions. In this work, we applied high-level quantum calculation and Transition State Theory (TST) to predict ΔG_{gas}. We also used boxed molecular dynamics (Boxed MD, BXD)[59-61] to evaluate PMF in solvent and gas phases, and calculate their difference $\Delta\Delta G_{sol}$. BXD is the accelerated sampling technique for description of rare events and calculation of PMF. In BXD, the reaction coordinate r is divided into several "boxes" so that all the events can be considered in

each box. The dynamics is "locked" within each box by means of inverting the velocity of the trajectory when the reaction coordinate *r* reaches the edge of each box. After sufficient number of events is collected, the system is allowed to move to the next box. The rate constant *k* between boxes can be therefore calculated from the average time between the hits:

$$k_{m,m\pm1} = \frac{h_{m,m\pm1}}{t_m} \quad (5)$$

where $h_{m,m\pm1}$ is the number of hits of the boundary of the *m*th box and t_m is the time spent in the box. The assumption of BXD is that the sequential hits and velocity inversion is uncorrelated. Unlike umbrella sampling (US) technique[62] for the evaluation of free energy, BXD does not employ any bias potential.

To the best of our knowledge, this work represents the first theoretical investigation of the rate constant of R1 and R1r in extremely high pressure in sCO_2 environment. Instead of QM/MM[63] with semi-empirical correction by London, Eyring, Polanyi, and Sato (LEPS)[64-65] used in our previous publications,[19-21] here we applied multi-state empirical valence bond (MS-EVB)[66-67] method to obtain more accurate PES. MS-EVB reproduces reactive potential surface in the transition state and post-transition state regions and bridges the gap between quantum and classical mechanics.

Computational Methods

Coupled cluster with singles and doubles substitutions method CCSD[68-70] in conjunction with Dunning's correlation consistent basis set cc-pVTZ[71-72] was selected for geometry optimization and vibrational analysis of C_2H_6 (D_{3d} symmetry) and CH_3 (D_{3h} symmetry). C_2H_6 transition state was determined by canonical variational TST (CVTST)[43, 45] since the reaction has

no well-defined TS (simple bond-breaking reaction). Several non-stationary structures were optimized with constrained bond lengths. The structure with the highest Gibbs energy along the reaction path (C-C bond) was taken to be the generalized TS. In this study, the TS bond length was 2.70 Å in 2000 K with D_{3d} symmetry. All QM calculations were performed with Gaussian09 Program.[73] GPOP (Gaussian Post Processor) program,[74] which implements rigid rotor/harmonic oscillator approximation and hindered internal rotor, was used to calculate equilibrium constant K_{eq} and microscopic rate constants k. $\Delta G_{gas}(r)$ was obtained from Eq.2 after rate constant k was evaluated by GPOP. $\Delta\Delta G_{sol}(r)$ was obtained from PMF obtained in classical MD simulations. All the MD calculations were performed with CHARMM (version c42b1).[75-76] MS-EVB[66-67] approach was used to describe PES of the reactive system: C_2H_6 and CH_3 force fields (Figure 2) were redesigned using experimental bong lengths and vibrational frequencies values in NIST database.[77] CO_2 force field is TraPPE-flex[78] (flexible molecule version of TraPPE).[79-80] These bond and no-bond covalent states form the basis to describe Hamiltonian matrix H(q):

$$H(q) = \begin{bmatrix} V_R + \varepsilon_R & H_{12} \\ H_{12} & V_P + \varepsilon_P \end{bmatrix} \quad (6)$$

where ε_R = -96.0 and ε_P = 2.0 represent constant diagonal energy shifts (R denotes reactant and P denotes product). The diagonal elements V_R and V_P correspond to the molecular mechanics energy of particular molecular valence states (Figure 2). The off-diagonal $H_{12}(r_1,r_2)$ was fitted from two-dimensional ellipsoid Gaussian function:

$$H_{12}(r_1,r_2) = A_{12}\exp\left(-a(r_1 - r_1^0)^2 + 2b(r_1 - r_1^0)(r_2 - r_2^0) + c(r_2 - r_2^0)^2\right) \quad (7)$$

where r_1 and r_2 are the C-C bond distance in stable and transition states, A_{12} = 80.0 is the Gaussian amplitude, and r_1^0 = 1.5 Å and r_2^0 = 4.5 Å are the respective reference values of r_1 and r_2. a, b, and c are defined as:

$$a = \frac{cos^2\theta}{2\sigma_{r_1}^2} + \frac{sin^2\theta}{2\sigma_{r_2}^2} \quad (8)$$

$$b = -\frac{sin2\theta}{4\sigma_{r_1}^2} + \frac{sin2\theta}{2\sigma_{r_2}^2} \quad (9)$$

$$c = \frac{sin^2\theta}{2\sigma_{r_1}^2} + \frac{cos^2\theta}{2\sigma_{r_2}^2} \quad (10)$$

where θ is the Gaussian rotation angle, and $\sigma_{r1} = 7.5$, $\sigma_{r2} = 10.0$ are the respective widths in the r_1 and r_2 directions. The shifted energy ε_R and ε_P, the amplitude A_{12}, the centers r_1^0 and r_2^0, and the widths σ_{r1} and σ_{r2} were tuned to adjust PES to be comparable to high-level quantum simulation. In our case, CASPT2 calculation was used as benchmark PES to mimic[46] (see Figure S1 in Supporting Information).

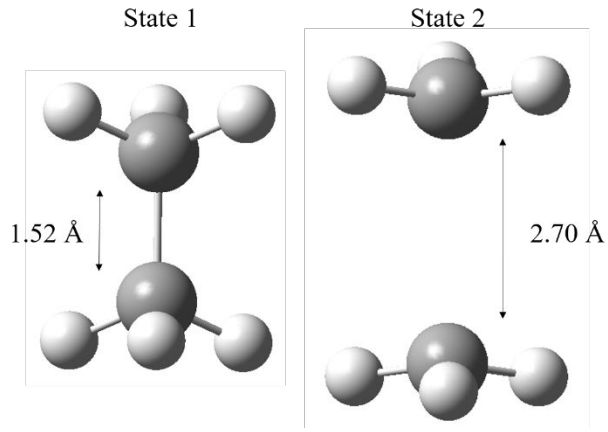

Figure 2. Schematic representation of the two covalent states (reactant and product) in the MS-EVB model.

The simulation system was equilibrated for 4 ns, followed by 4 to 6 ns production run. MD simulations were performed for constant volume and temperature ensemble (*NVT*). Nose-Hoover[81-82] thermostat was combined with velocity-Verlet integrator. Relatively short 0.2 fs time

step was applied to describe light H atom motion. Periodic boundary condition (PBC) in cubic 26.0*26.0*26.0 Å^3 unit cell with particle mesh Ewald (PME)[83-84] summation were used to better estimate long-range interactions. The simulation cell includes one C_2H_6 and *N* CO_2 molecules (*N* = 0, 2, 4, 8, 16, 32, and 77). The trajectories were collected for the temperatures of 1000, 1200, 1400, 1600, 1800, and 2000 K.

Accelerated MD approach BXD,[59-61] implemented in AXD module of CHARMM was applied for rare events of C-C bond breaking and forming. The reaction coordinate C-C bond distance was assigned in the range from 1.4 to 8.0 Å and was divided into intervals (boxes) 0.05 Å wide (from 1.4 to 3.5 Å), 0.1 Å wide (from 3.5 to 4.0 Å), 0.2 Å wide (from 4.0 to 6.0 Å), and 1.0 Å wide (from 6.0 to 8.0 Å). There were 59 boxes in total. The selection of the size of each box is important so that the box is big enough to avoid ballistic reflection and small enough so that reactive events are collected at the boundaries for further box-averaged free energy. As the gradient is steeper, smaller boxes are chosen, and *vice versa*. The MD trajectory is propagated until reaction coordinate exceeds the limit of the box. The velocity of the two atoms involved are inverted in the direction of the reaction coordinate. After the reflection event occurred 500 times, the system is allowed to cross the boundary to the adjacent box. The simulation continued until 10 to 30 passes were made. The trajectories of reaction coordinate ρ was collected to convert into free energy profile $G(\rho)$ and PMF was obtained:

$$p(r) = \frac{\exp\left(-\frac{G(\rho)}{kT}\right)}{\int \exp\left(-\frac{G(\rho)}{kT}\right) d\rho}. \quad (11)$$

Eyring-Polanyi equation Eq.4 was then employed to predict rate constant based upon PMF. Tabulated values for rate constant were interpolated to 30, 100, 300, and 1000 atm and fitted by linear least square regression model in Arrhenius eq. 12 or extended Arrhenius eq. 13:

$$k = Aexp(-\frac{E_a}{RT}) \quad (12)$$

where A is pre-exponential factor and E_a is phenomenological activation energy, and

$$k = AT^n \exp(-\frac{E_a}{RT}) \quad (13)$$

where n is empirical constant (restrained within $|n| \leq 1$).

Results and Discussion

Dissociation $C_2H_6 \rightarrow CH_3 + CH_3$ in Gas Phase The rate constant k of ethane dissociation at high-pressure limit is performed by TST by CCSD/cc-pVTZ method. The calculated k of R1 in the assigned temperatures and the Arrhenius equation parameters are listed in Table 1. A, n, and E_a are temperature-independent and k is temperature-dependent. k in different temperature increases significantly by the order of 3. Positive E_a (~88 kcal/mol) describes the energy barrier of bond dissociation and is close to the activation energy obtained experimentally.[47-48]

Table 1. Rate constant k of R1 (1/s) reaction and the Arrhenius equation parameters

		Arrhenius equation		Extended Arrhenius equation		
T	k	A	E_a	A	N	E_a
K	1/s	1/s	cal/mol	1/s		cal/mol
1000	2.01E-05					
1200	3.58E-02					
1400	7.62E+00	7.22E+14	89493.3	3.03E+13	0.38	88441.9
1600	4.27E+02					
1800	9.84E+03					
2000	1.21E+05					

The rate constants k from extended Arrhenius equation between 1000 K and 2000 K are compared with other shock tube experiments in low pressure in Figure 3. The fitted k is located

slightly lower than other experimental results and as the temperature increases, *k* increases. Since Arrhenius equation and extended Arrhenius equation have nearly identical results, result from Arrhenius equation is not shown in Figure 3.

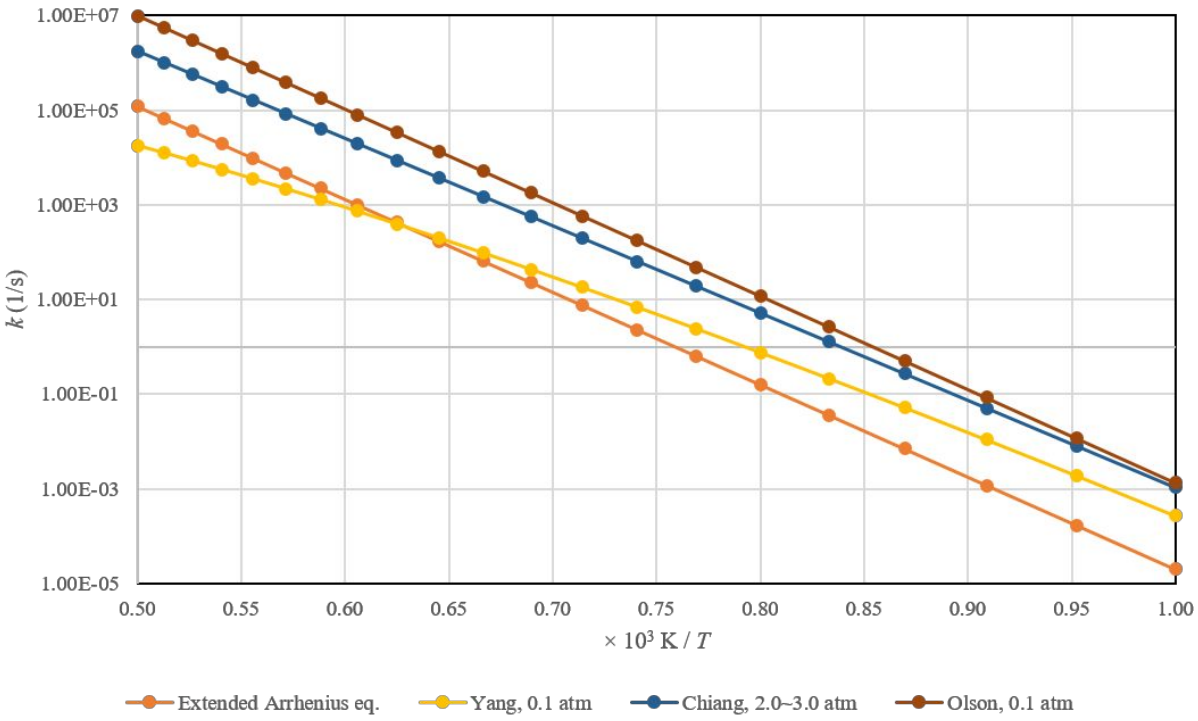

Figure 3. Arrhenius plot for R1 from extended Arrhenius equation compared with shock tube experiments from Yang[29] (0.08 atm), Chiang[32] (2.00 ~ 3.00 atm), and Olson[33] (0.03 ~ 0.11 atm) in low pressure.

In addition, other shock tube experiments[28, 30-31, 34] and theoretical studies including RRKM,[36] CASPT2//CASSCF,[46] and CR-CC(2,3)//MP2[49] shows one order higher rate constant than experiments on average (see Table S1-1 and S1-2 in Supporting Information).

Dissociation $C_2H_6 \rightarrow CH_3 + CH_3$ in Solvent Phase The reaction R1 in sCO_2 environment was performed at various number of CO_2 molecules in *NVT* ensemble and corresponds to various

pressures. Figure 4 shows the representative snapshots of C_2H_6 molecules in sCO_2 environment. As the number of CO_2 molecule increases, the system approaches homogeneity. The example of PMF of dissociation reaction is shown in Figure S2 (see Supporting Information). As the number of CO_2 molecules increases, the free energy barrier of R1 decreases.

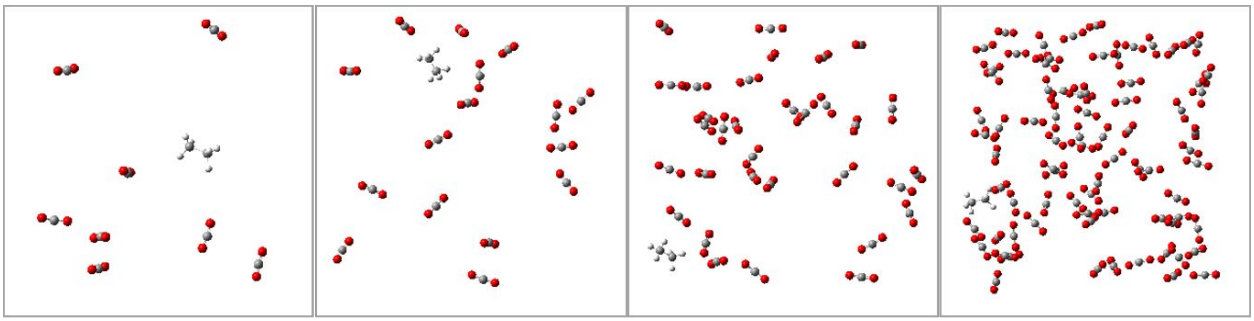

Figure 4. Representative snapshot of C_2H_6 molecules in sCO_2 environment from 8 to 77 CO_2 molecules.

The MD correction $\Delta\Delta G_{sol}$ is calculated as $\Delta G_{sol}(N\ CO_2)$ - $\Delta G_{sol}(0\ CO_2)$ (N = 2, 4, 8, 16, 32, or 77) from PMF. Table S2 lists the pressures at different densities (number of CO_2 molecules) and temperatures. The increase of temperature leads to pressure increase. As the number of CO_2 molecules increases, the pressure increase becomes more significant. When N = 8, both temperature and pressure reach supercritical condition. The MD corrected $\Delta G^{\ddagger}$ is therefore calculated by adding MD correction $\Delta\Delta G_{sol}$ to ΔG_{gas} reported in the previous section. These values were used to predict rate constant k with Eq. 3 & 4 at various N and shown in Table S3. As N increases, $\Delta G^{\ddagger}$ increases and k decreases. Decrease of $\Delta G^{\ddagger}$ and increase of k as N increases is more significant at 1,000 K than at 2,000 K. As T increase, $\Delta G^{\ddagger}$ decreases and k increases. In summary, as the pressure and temperature increase, the rate constant of R1 increases.

To investigate the pressure points of interests (30, 100, 300, and 1000 atm), the corresponding rate constant *k* is estimated by linear interpolation and collected in Table S4. Figure S3 shows the rate constant *k* in gas phase and the pressure 30, 100, 300, and 1000 atm. The higher the pressure, the higher *k* is. At lower temperature 1000 K, *k* difference is more significant. At higher temperature 2000 K, *k* at different pressures becomes closer to each other (converges at high temperature).

Table 2 shows the parameters of Arrhenius equation and extended Arrhenius equation. The best fit of *n* in extended Arrhenius equation is located at $|n| < 1.0$. The activation energy E_a fitted by Arrhenius and extended Arrhenius equations are in the range of 72~81 kcal/mol and it represents the activation barrier, typical for endothermic bond breaking. As the pressure increases, E_a decreases consistently. Parameters *A* and *n* in extended Arrhenius equation show more significant differences while E_a is still consistent with the endothermic nature of the dissociation reaction R1.

Table 2. Fitted Arrhenius equation and extended Arrhenius equation of R1 between 1000 and 2000 K

		Arrhenius equation Pressure (atm)				Extended Arrhenius equation Pressure (atm)			
		30	100	300	1000	30	100	300	1000
A	1/s	9.33E+13	5.46E+13	4.50E+13	1.53E+13	6.93E+3	7.01E+6	2.41E+14	3.52E+1
n		0	0	0	0	2.82	1.92	-0.20	3.25
E_a	cal/mol	81287.4	77958.7	76469.8	72346.9	73550.7	72694.9	77025.9	63476.3

Since the parameters of Arrhenius equation lead to similar results, only extended Arrhenius equation fitted result is shown in Figure 5. The higher the pressure and temperature, the higher the rate constant *k*. At higher temperature, *k* for different pressures are closer to each other, than those

at lower temperatures. The pressure of interest for Allam Cycle is 300 atm and k at 1000 K is 8.65×10^{-4} 1/s, while at 2000 K it is 1.97×10^{5} 1/s.

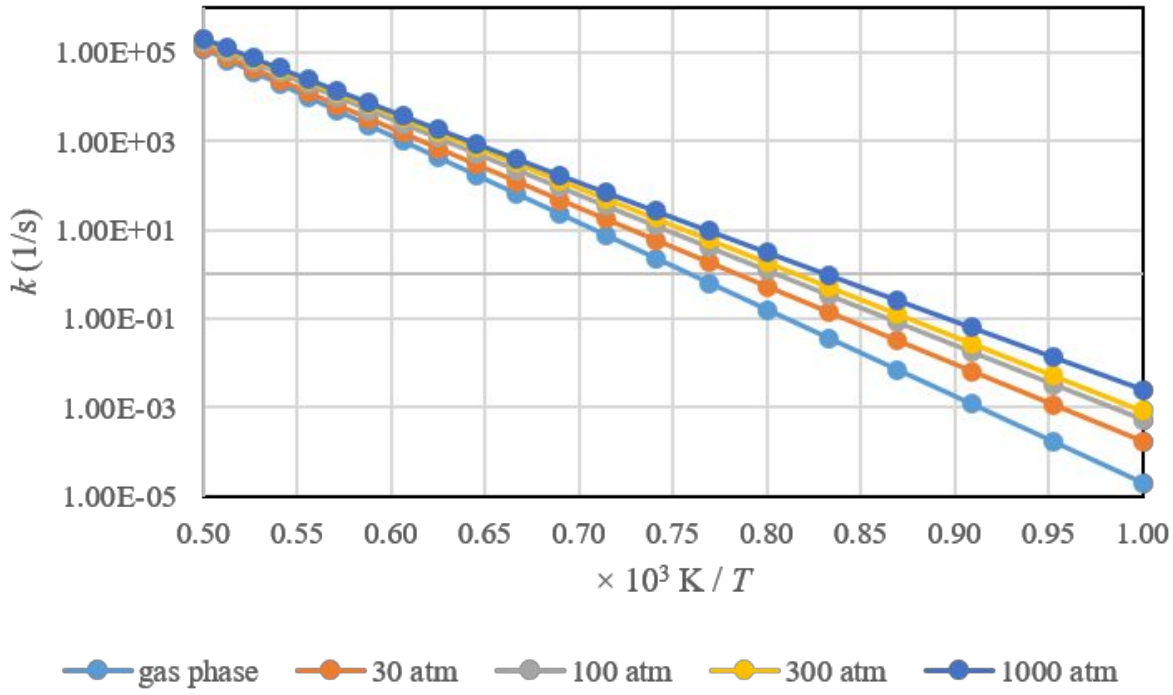

Figure 5. Rate constant k of R1 fitted by extended Arrhenius equation in gas phase and at the pressure of 30, 100, 300, and 1000 atm

Recombination $CH_3 + CH_3 \rightarrow C_2H_6$ in Gas Phase The CCSD/cc-pVTZ calculated rate constants k for methyl-methyl recombination and the parameters of Arrhenius equation and extended Arrhenius equation are shown in Table 3. Unlike R1, the range of k of R1r is narrow (10^{-12}~10^{-11}). This brought the significant difference of Arrhenius factor A between Arrhenius and extended Arrhenius equations (10^{-12} and 10^{-21}). Both E_a are negative with ~6.4 kcal/mol difference.

Table 3. Rate constant *k* of R1r reaction and the Arrhenius equation parameters.

		Arrhenius equation		Extended Arrhenius equation		
T	*k*	*A*	E_a	*A*	*n*	E_a
K	cm^3/molecule/s	cm^3/molecule/s	cal/mol	cm^3/molecule/s		cal/mol
1000	1.69E-11					
1200	1.02E-11					
1400	7.56E-12	1.51E-12	-4665.5	5.64E-21	2.35	-11101.9
1600	6.27E-12					
1800	5.61E-12					
2000	5.27E-12					

Figure 6 presents the comparison of rate constant *k* of R1r of this work and with AramcoMech 2.0,[26] laser photolysis,[42] shock tube[35] experiments, RRKM theory,[56] and Monte Carlo simulation.[57] The recombination rate constant *k* varies from 10^{-11} (AramcoMech2.0,[26] Du,[42] and Wagner[56]) to 10^{-12} (this work, Hessler,[57] and Möller[35]), illustrating the difficulty to evaluate an accurate *k*.

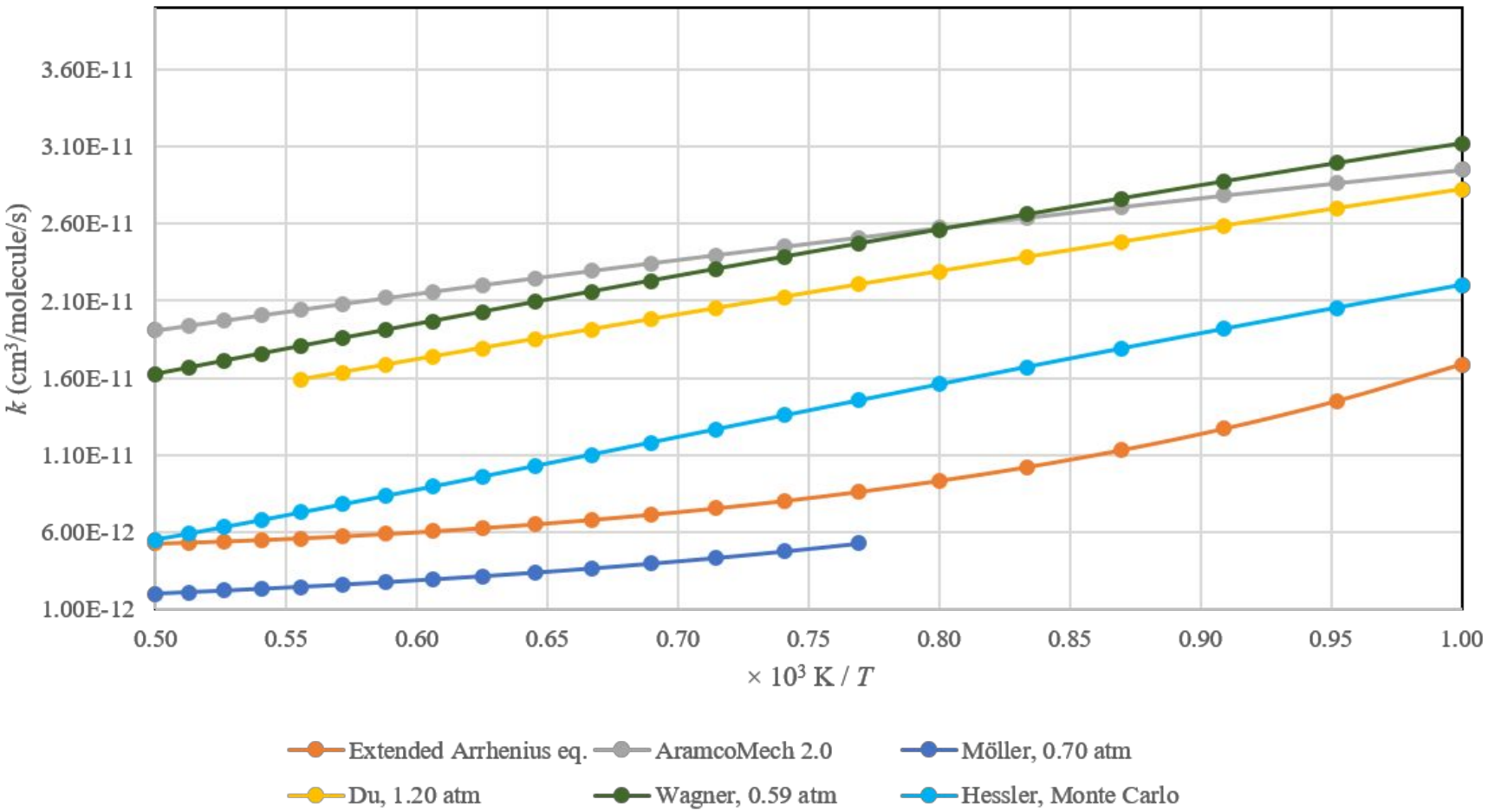

Figure 6. Rate constant k (cm^3/molecule/s) of R1r from extended Arrhenius equation compared with AramcoMech 2.0[26] and shock tube experiments from Du[42] (1.20 atm), Möller[35] (0.70 atm) in low pressure as well as theory from Wagner[56] (0.59 atm) and Hesler.[57]

Results of other theoretical calculations, including MRCI//CASSCF,[39] CASPT2(2,2)//CASSCF,[46] M06-L,[52] Master equation,[54-55] Monte Carlo,[48, 57] and CASPT2//B3LYP[51] were tabulated in Table S5 (see Supporting Information). The slight difference of fitted *k* between Arrhenius equation and extended Arrhenius equation is observed. The discrepancy of *k* between different measurements remain.

Recombination $CH_3 + CH_3 \rightarrow C_2H_6$ in Solvent Phase The activation free energies for the reaction R1r in sCO_2 environment at various temperatures and numbers of CO_2 molecules in *NVT* ensemble were predicted with Eq. 3, and rate constants were calculated with Eq. 4. Table S6 lists $\Delta G^{\ddagger}$ and *k* of R1r at $N = 0$ to 77. The value of $\Delta G^{\ddagger}$ is smaller than in R1, consistent with the lower free energy barrier for methyl-methyl recombination reaction. As *T* increases, $\Delta G^{\ddagger}$ increase and *k* decreases. As *N* increases, $\Delta G^{\ddagger}$ decreases and *k* increases. In this reaction, lower *T* with higher *N* lead to higher *k* and *vice versa*. The rate constants in solvent phase and fixed pressures 30, 100, 300, and 1000 atm were estimated by the linear interpolation and collected in Table S7. At supercritical CO_2 condition (100, 300, and 1000 atm), *k* is higher than in 30 atm. Figure S4 presents the Arrhenius plot for R1r rate constant *k* in gas and solvent phase at 30, 100, 300, and 1000 atm. The rate constant *k* in solvent phase is always higher than in gas phase. The slope of the Arrhenius plots in the solvent phase is larger than in the gas phase indicating that the reaction R1r is more temperature-sensitive than of R1 at high pressure.

Table 4 represents the Arrhenius and extended Arrhenius equation parameters. As the pressure increases, the effective energy barrier E_a decreases from -12 to -20 kcal/mol. Negative sign indicates that methyl-methyl recombination slows down with increasing temperature.

Table 4. Fitted Arrhenius equation and extended Arrhenius equation of R1r between 1000 and 2000 K.

		Arrhenius equation Pressure (atm)				Extended Arrhenius equation Pressure (atm)			
		30	100	300	1000	30	100	300	1000
A	cm^3/molecule/s	2.09E-13	1.11E-13	1.01E-13	3.05E-13	1.44E-28	1.31E-27	8.44E-19	3.16E-40
n		0	0	0	0	4.23	3.88	1.42	7.25
E_a	cal/mol	-12359.8	-15154.0	-16008.0	-20114.0	-23940.5	-25792.0	-19887.0	-39960.5

Figure 7 shows the relationship of k of R1r fitted by extended Arrhenius equation. k in 300 atm is of our interest for Allam Cycle that in 1000 K, k is 3.3×10^{-10} cm^3/molecule/s and in 2000 K, k is 6.0×10^{-12} cm^3/molecule/s. The gradient increases as the pressure increases if the temperature is lower. In 2000 K, the rate constant k has limited difference no matter how high the pressure is, which shows k convergence of R1r as k of R1.

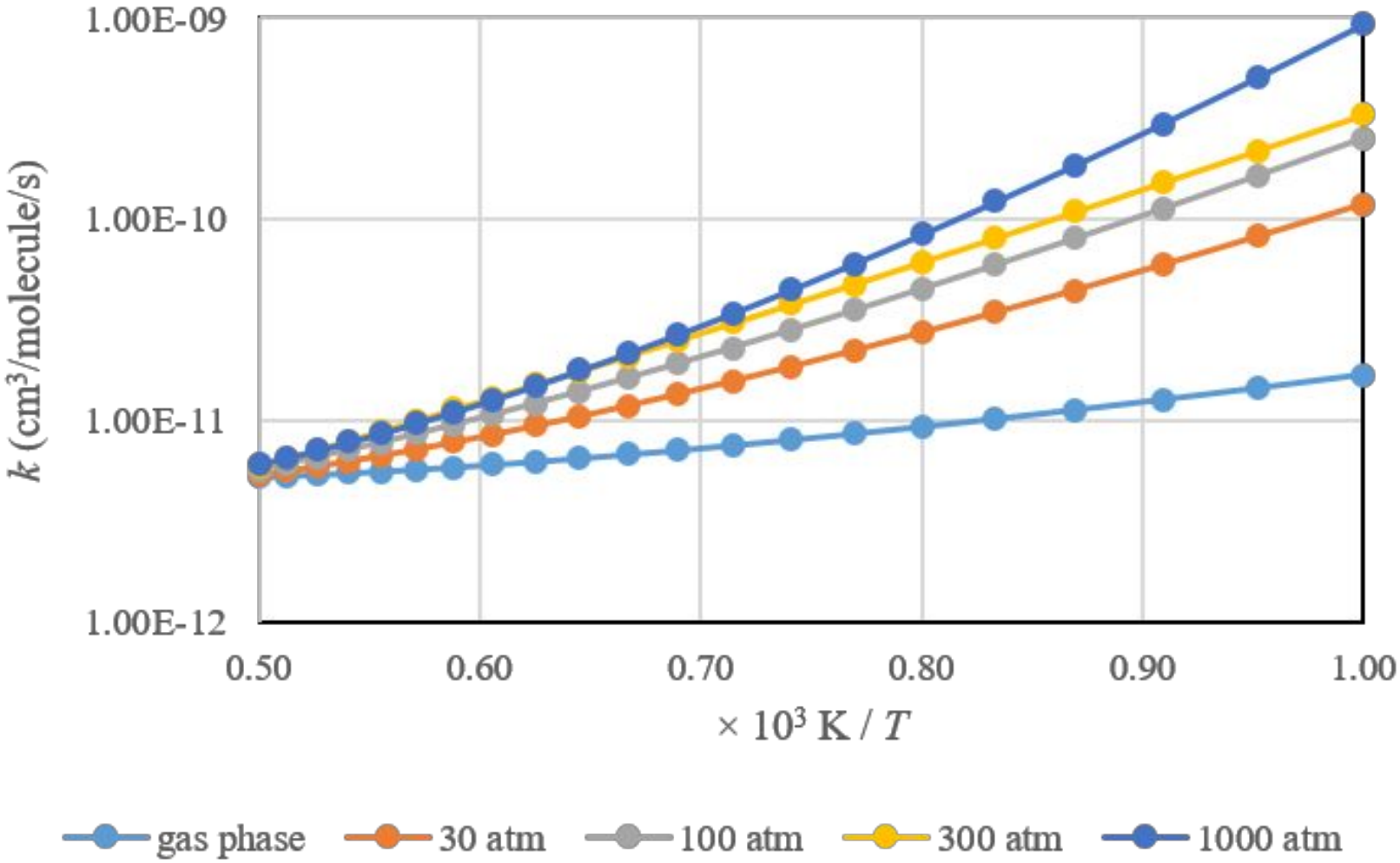

Figure 7. Rate constant *k* of R1r in gas and solvent phase 30, 100, 300, and 1000 atm fitted by extended Arrhenius equation

Conclusions

We have successfully simulated reaction $C_2H_6 \rightleftharpoons CH_3 + CH_3$ in supercritical CO_2 environment and evaluated the rate constants k in high temperatures and pressures. In sCO_2 environment, k of R1 and R1r increase monotonically as the pressure increases. Compared with k in the gas phase, at 1000K and 300 atm, (1) the rate constant of R1 is significantly higher (2.0×10^{-5} vs. 8.7×10^{-4} 1/s), while at 2000 K the rate constants become closer (1.2×10^{5} vs. 2.0×10^{5} 1/s); (2) the rate constant of R1r is significantly higher (1.6×10^{-11} vs. 3.3×10^{-10} cm^3/molecule/s), while at 2000 K the rate constant is converged to $5.0\times10^{-12} \sim 5.9\times10^{-12}$ cm^3/molecule/s. Our predictions of k at 300 atm and parameters of Arrhenius equation for the radical chain termination pressure-dependent methyl-methyl recombination in methane combustion pathways will help more accurate description of Allam cycle. This study also introduced an important methodology that can be applied to other combustion reactions of oxy-fuel power cycle at high temperatures and pressures. This method includes evaluation of PMF in gas and solvent (sCO_2) phases by accelerated MD simulations, estimation of free energy barriers for both phases, and calculating MD correction by taking their difference. This MD correction is then added to free energy barriers obtained in quantum mechanical treatment used in TST. The method also includes MS-EVB treatment for accurate representation of the potential energy surface for free radical reaction and application of BXD for the exploration of rare events of bond breaking to calculate accurate free energy profiles. There are other combustion reactions in sCO_2 environment are presently under study. Other kinetics discussion of bimolecular reactions can be found in Fernández-Ramos et al.[85]

Associated Content

Supporting Information

The Supporting Information is available free of charge on the ACS Publications website at DOI:xxxxxxxx:

Potential energy surface, rate constants at various temperatures, potential of mean force, calculated density and pressure of the MD simulation, free energy and rate constants corresponding to various densities of CO_2 (PDF)

Author Information

Corresponding Authors

*(A.E.M.) E-mail: amasunov@ucf.edu; (S.S.V.) E-mail: subith@ucf.edu

ORCID

Chun-Hung Wang: 0000-0002-0223-2695

Sergey V. Panteleev: 0000-0001-8780-5642

Artëm E. Masunov: 0000-0003-4924-3380

Subith S. Vasu: 0000-0002-4164-3163

Acknowledgements

This contribution is based upon work supported by KEPCO Research Institute (KEPRI), Hanhwa Power Systems (HPS), and Southwest Research Institute (SwRI). Partially financial support from UCF College of Graduate Studies is appreciated. The authors also acknowledge the National Energy Research Scientific Computing Center (NERSC), and the University of Central Florida

Advanced Research Computing Center (https://arcc.ist.ucf.edu) for providing computational resources and support. A.E.M. acknowledges support by the Act 211 Government of the Russian Federation (contract no. 02.A03.21.0011) and by the "improving of the competitiveness" program of the National Research Nuclear University MEPhI.

References

1. Figueroa, J. D.; Fout, T.; Plasynski, S.; McIlvried, H.; Srivastafa, R. D., Advances in CO_2 capture technology - The U.S. Department of Energy's Carbon Sequestration Program. *International Journal of Greenhouse Gas Control* **2008,** *2* (1), 9-20.
2. Yang, H.; Xu, Z.; Fan, M.; Gupta, R.; Slimane, R. B.; Bland, A. E.; Wright, I., Progress in carbon dioxide separation and capture: A review. *Journal of Environmental Sciences* **2008,** *20*, 14-27.
3. Buhre, B. J. P.; Elliott, L. K.; Sheng, C. D.; Gupta, R. P.; Wall, T. F., Oxy-fuel combustion technology for coal-fired power generation. *Progress in Energy and Combustion Science* **2005,** *31*, 283-307.
4. Allam, R.; Martin, S.; Forrect, B.; Fetvedt, J.; Lu, X.; Freed, D.; Brown, G. W., Jr.; Sasaki, T.; Itoh, M.; Manning, J., Demonstration of the Allam Cycle: An Update on the Development Status of a High Efficiency Supercritical Carbon Dioxide Power Process Employing Full Carbon Capture. *Energy Procedia* **2017,** *114*, 5948-5966.
5. Scaccabarozzi, R.; Gatti, M.; Martelli, E., Thermodynamic analysis and numerical optimization of the NET Power oxy-combustion cycle. *Applied Energy* **2016,** *178*, 505-526.
6. Laumb, J. D.; Holmes, M. J.; Stanislowski, J. J.; Lu, X.; Forrest, B.; McGroddy, M., Supercritical CO2 cycles for power production. *Energy Procedia* **2017,** *114*, 573-580.
7. Lu, X.; Martin, S.; McGroddy, M.; Swanson, M.; Stanislowski, J.; Laumb, J. D., Testing of a Novel Post Combustion Acid Removal Process for the Direct-Fired, Oxy-Combustion Allam Cycle Power Generation System. *Journal of Engineering for Gas Turbines and Power-Transactions of the ASME* **2018,** *140*, 081701.
8. Allam, R. J.; Fetvedt, J. E.; Forrest, B. A.; Freed, D. A., The Oxy-Fuel, Supercritical CO_2 Allam Cycle: New Cycle Developments to Produce Even Lower-Cost Electricity From Fossil Fuels Without Atmospheric Emissions. *The American Society of Mechanical Engineers. Turbo Expo: Power for Land, Sea, and Air* **2014,** *3B: Oil and Gas Applications; Organic Ranking Cycle Power Systems; Supercritical CO2 Power Cycles; Wind Energy*, V03BT36A016.
9. Manikantachari, K. R. V.; Martin, S.; Bobren-Diaz, J. O.; Vasu, S. S., Thermal and Transport Properties for the Simulation of Direct-Fired sCO_2 Combustor. *Journal of Engineering for Gas Turbines and Power* **2017,** *139* (12), 121505.
10. Manikantachari, K. R. V.; Vesely, L.; Martin, S.; Bobren-Diaz, J. O.; Vasu, S. S., Reduced Chemical Kinetic Mechanisms for Oxy/Methane Supercritical CO_2 Combustor Simulations. *Journal of Energy Resources Technology-Transactions of the ASME* **2018,** *140* (9), 092202.
11. Manikantachari, K. R. V.; Martin, S.; Rahman, R. K.; Velez, C.; Vasu, S. S. In *A General Study of Counterflow Diffusion Flames for Supercritical CO_2 Mixtures*, Proceedings of the ASME Turbo Expo 2019: Turbomachinery Technical Conference & Exposition, Phoenix, AZ, Phoenix, AZ, 2019; pp GT2019-90332.
12. Masunov, A. E.; Atlanov, A. A.; Vasu, S. S., Potential Energy Surfaces for the Reactions of HO2 Radical with CH_2O and HO_2 in CO_2 Environment. *Journal of Physical Chemistry A* **2016,** *120* (39), 7681-7688.

13. Masunov, A. E.; Wait, E.; Vasu, S. S., Chemical Reaction CO+OH→CO_2+H-center dot Autocatalyzed by Carbon Dioxide: Quantum Chemical Study of the Potential Energy Surfaces. *Journal of Physical Chemistry A* **2016,** *120* (30), 6023-6028.
14. Masunov, A. E.; Wait, E.; Vasu, S. S., Quantum Chemical Study of CH3 + O-2 Combustion Reaction System: Catalytic Effects of Additional CO_2 Molecule. *Journal of Physical Chemistry A* **2017,** *121* (30), 5681-5689.
15. Masunov, A. E.; Wait, E. E.; Atlanov, A. A.; Vasu, S. S., Quantum Chemical Study of Supercritical Carbon Dioxide Effects on Combustion Kinetics. *Journal of Physical Chemistry A* **2017,** *121* (19), 3728-3735.
16. Masunov, A. E.; Wait, E. E.; Vasu, S. S., Catalytic Effect of Carbon Dioxide on Reaction OH plus CO → H + CO_2 in Supercritical Environment: Master Equation Study. *Journal of Physical Chemistry A* **2018,** *122* (31), 6355-6359.
17. Wait, E. E.; Masunov, A. E.; Vasu, S. S., Quantum chemical and master equation study of OH + CH_2O → H_2O + CHO reaction rates in supercritical CO_2 environment. *International Journal of Chemical Kinetics* **2019,** *51* (1), 42-48.
18. Masunov, A. E.; Atlanov, A. A.; Vasu, S. S., Molecular Dynamics Study of Combustion Reactions in a Supercritical Environment. Part 1: Carbon Dioxide and Water Force Field Parameters Refitting and Critical Isotherms of Binary Mixtures. *Energy & Fuels* **2016,** *30* (11), 9622-9627.
19. Panteleev, S. V.; Masunov, A. E.; Vasu, S. S., Molecular Dynamics Study of Combustion Reactions in a Supercritical Environment. Part 2: Boxed MD Study of CO + OH → CO2 + H Reaction Kinetics. *The Journal of Physical Chemistry A* **2018**.
20. Panteleev, S. V.; Masunov, A. E.; Vasu, S. S., Molecular Dynamics Study of Combustion Reactions in Supercritical Environment. Part 3: Boxed MD Study of CH_3 + HO_2 → CH_3O + OH Reaction Kinetics. *Journal of Physical Chemistry A* **2018,** *122*, 3337-3345.
21. Panteleev, S. V.; Masunov, A. E.; Vasu, S. S., Molecular dynamics of combustion reactions in supercritical carbon dioxide. Part 4: boxed MD study of formyl radical dissociation and recombination. *Journal of Molecular Modeling* **2019,** *25*, 35.
22. Warnatz, J., Hydrocarbon oxidation high-temperature chemistry. *Pure and Applied Chemistry* **2000,** *72* (11), 2101-2110.
23. Rabitz, H.; Kramer, M.; Dacol, D., Sensitivity Analysis in Chemical Kinetics. *Annual Review of Physical Chemistry* **1983,** *34*, 419-461.
24. Atherton, R. W.; Schainker, R. B.; Ducot, E. R., On the statistical sensitivity analysis of models for chemical kinetics. *AIChE Journal* **1975,** *21* (3), 441-448.
25. CHEMKIN-PRO 15131 Reaction Design: San Diego. **2013**.
26. Metcalfe, W. K.; Burke, S. M.; Ahmed, S. S.; Curran, H. J., A Hierarchical and Comparative Kinetic Modeling Study of C1-C2 Hydrocarbon and Oxygenated Fuels. *International Journal of Chemical Kinetics* **2013,** *45* (10), 638-675.
27. Yao, Q.; Cao, X.-M.; Zong, W.-G.; Sun, X.-H.; Li, Z.-R.; Li, X.-Y., Potential Energy Surface for Large Barrierless Reaction Systems: Application to the Kinetic Calculations of the Dissociation of Alkanes and the Reverse Recombination Reactions. *Journal of Physical Chemistry A* **2018,** *122*, 4869-4881.
28. Oehlschlaeger, M. A.; Davidson, D. F.; Hanson, R. K., High-temperature ethane and propane decomposition. *Proceedings of the Combustion Institute* **2005,** *30*, 1119-1127.
29. Yang, X.; Jasper, A. W.; Kiefer, J. H.; Tranter, R. S., The Dissociation of Diacetyl: A Shock Tube and Theoretical Study. *Journal of Physical Chemistry A* **2009,** *113*, 8318-8326.
30. Hidaka, Y.; Shiba, S.; Takuma, H.; Suga, M., Thermal decomposition of ethane in shock waves. *International Journal of Chemical Kinetics* **1985,** *17* (4), 441-453.
31. Burcat, A.; Skinner, G. B.; Crossley, R. W.; Scheller, K., High temperature decomposition of ethane. *International Journal of Chemical Kinetics* **1973,** *5* (3), 345-352.

32. Chiang, C.-C.; Skinner, G. B., Resonance Absorption Measurements of Atom Concentrations in Reacting Gas Mixtures. 7. Pyrolysis of C_2H_6 and C_2D_6 Behind Shock Waves. *Journal of Physical Chemistry* **1981,** *85*, 3126-3129.
33. Olson, D. B.; Gardiner, W. C., Jr., Thermal Dissociation Rate of Ethane at the High Pressure Limit from 250 to 2500 K. *Journal of Physical Chemistry* **1979,** *83* (8), 922-927.
34. Davidson, D. F.; Di Rosa, M. D.; Hanson, R. K.; Bowman, C. T., A study of ethane decomposition in a shock tube using laser absorption of CH_3. *International Journal of Chemical Kinetics* **1993,** *25* (11), 969-982.
35. Möller, W.; Mozzhukhin, E.; Wagner, H. G., High Temperature Reactions of CH_3 1. The Reaction CH3 + H2 -> CH4 + H. *Berichte der Bunsengesellschaft für Physikalische Chemie* **1986,** *90*, 854-861.
36. Kiefer, J. H.; Santhanam, S.; Srinivasan, N. K.; Tranter, R. S.; Klippenstein, S. J.; Oehlschlaeger, M. A., Dissociation, relaxation, and incubation in the high-temperature pyrolysis of ethane, and a successful RRKM modeling. *Proceedings of the Combustion Institute* **2005,** *2005*, 1129-1135.
37. Yang, X.; Goldsmith, C. F.; Tranter, R. S., Decomposition and Vibrational Relaxation in CH3I and Self-Reaction of CH3 Radicals. *Journal of Physical Chemistry A* **2009,** *113*, 8307-8317.
38. Davidson, D. F.; Di Rosa, M. D.; Chang, E. J.; Hanson, R. K.; Bowman, C. T., A Shock Tube Study of Methyl-Methyl Reactions between 1200 and 2400 K. *International Journal of Chemical Kinetics* **1995,** *27*, 1179-1196.
39. Wang, B.; Hou, H.; Yoder, L. M.; Muckerman, J. T.; Fockenberg, C., Experimental and Theoretical Investigations on the Methyl-Methyl Recombination Reaction. *Journal of Physical Chemistry A* **2003,** *107*, 11414-11426.
40. Slagle, I. R.; Gutman, D.; Davies, J. W.; Pilling, M. J., Study of the Recombination Reaction $CH_3 + CH_3 \rightarrow C_2H_6$. 1. Experiment. *Journal of Physical Chemistry* **1988,** *92*, 2455-2462.
41. Sangwan, M.; Yan, C.; Chesnokov, E. N.; Krasnoperov, L. N., Reaction $CH_3 + CH_3 \rightarrow C_2H_6$ Studied over the 292-714 K Temperature and 1-100 bar Pressure Ranges. *Journal of Physical Chemistry A* **2015,** *119*, 7847-7857.
42. Du, H.; Hessler, J. P.; Ogren, P. J., Recombination of Methyl Radicals. 1. New Data between 1175 and 1750 K in the Falloff Region. *Journal of Physical Chemistry* **1996,** *100*, 974-983.
43. Truhlar, D. G.; Garrett, B. C.; Klippenstein, S. J., Current Status of Transition State Theory. *Journal of Physical Chemistry* **1996,** *100*, 12771-12800.
44. Truhlar, D. G., Transition state theory for enzyme kinetics. *Archives of Biochemistry and Biophysics* **2015,** *582*, 10-17.
45. Bao, J. L.; Truhlar, D. G., Variational transition state theory: theoretical framework and recent developments. *Chemical Societry Reviews* **2017,** *46*, 7548-7596.
46. Li, H.; Chen, B.-Z.; Huang, M.-B., CASPT2 Investigation of Ethane Dissociation and Methyl Recombination Using Canonical Variational Transition State Theory. *International Journal of Chemical Kinetics* **2008,** *40*, 161-173.
47. Robertson, S. H.; Wardlaw, D. M.; Hirst, D. M., Potential energy function for $CH_3+CH_3 \rightarrow C_2H_6$: Attributes of the minimum energy path. *The Journal of Chemical Physics* **1993,** *99* (10), 7748-7761.
48. Pesa, M.; Pilling, M. J.; Robertson, S. H., Application of the Canonical Flexible Transition State Theory to CH_3, CF_3, and CCl_3 Recombination Reactions. *Journal of Physical Chemistry A* **1998,** *102*, 8526-8536.
49. Ge, Y.; Gordon, M. S.; Battaglia, F.; Fox, R. O., Theoretical Study of the Pyrolysis of Methyltrichlorosilane in the Gas Phase. 3. Reaction Rate Constant Calculations. *Journal of Physical Chemistry A* **2010,** *114*, 2384-2392.
50. Lorant, F.; Behar, F.; Goddard, W. A., III; Tang, Y., Ab Initio Investigation of Ethane Dissociation Using Generalized Transition State Theory. *Journal of Physical Chemistry A* **2001,** *105*, 7896-7904.
51. Klippenstein, S. J.; Georgievskii, Y.; Harding, L. B., Predictive theory for the combination kinetics of two alkyl radicals. *Physical Chemistry Chemical Physics* **2006,** *8*, 1133-1147.

52. Zheng, J.; Zhang, S.; Truhlar, D. G., Density Functional Study of Methyl Radical Association Kinetics. *Journal of Physical Chemistry A* **2008,** *112*, 11509-11513.
53. Golubeva, A. A.; Nemukhin, A. V.; Klippenstein, S. J.; Harding, L. B.; Krylov, A. I., Performance of the Spin-Flip and Multireference Methods for Bond Breaking in Hydrocarbons: A Benchmark Study. *Journal of Physical Chemistry A* **2007,** *111*, 13264-13271.
54. Blitz, M. A.; Green, N. J. B.; Shannon, R. J.; Pilling, M. J.; Seakins, P. W.; Western, C. M.; Robertson, S. H., Reanalysis of Rate Data for the Reaction $CH_3 + CH_3 \rightarrow C_2H_6$ Using Revised Cross Sections and a Linearized Second-Order Master Equation. *Journal of Physical Chemistry A* **2015,** *119*, 7668-7682.
55. Robertson, S. H.; Pilling, M. J.; Baulch, D. L.; Green, N. J. B., Fitting of Pressure-Dependent Kinetic Rate Data by Master Equation/Inverse Laplace Transform Analysis. *Journal of Physical Chemistry* **1995,** *99*, 13452-13460.
56. Wagner, A. F.; Wardlaw, D. M., Study of the Recombination Reaction $CH_3 + CH_3 \rightarrow C_2H_6$. 2. Theory. *Journal of Physical Chemistry* **1988,** *92*, 2462-2471.
57. Hessler, J. P.; Ogren, P. J., Recombination of methyl radicals .2. Global fits of the rate coefficient. *Journal of Physical Chemistry* **1996,** *100* (3), 984-992.
58. Akiya, N.; Savage, P. E., Effect of Water Density on Hydrogen Peroxide Dissociation in Supercritical Water. 2. Reaction Kinetics. *Journal of Physical Chemistry A* **2000,** *104*, 4441-4448.
59. Glowacki, D. R.; Paci, E.; Shalashilin, D. V., Boxed molecular dynamics: a simple and general technique for accelerating rare event kinetics and mapping free energy in large molecular systems. *Journal of Physical Chemistry B* **2009,** *113* (52), 16603-16611.
60. Glowacki, D. R.; Paci, E.; Shalashilin, D. V., Boxed molecular dynamics: decorrelation time scales and the kinetic master equation. *Journal of Chemical Theory and Computation* **2011,** *7* (5), 1244-1252.
61. Booth, J.; Vazquez, S.; Martinez-Nunez, E.; Marks, A.; Rodgers, J.; Glowacki, D. R.; Shalashilin, D. V., Recent applications of boxed molecular dynamics: a simple multiscale technique for atomistic simulations. *Philosophical Transactions of the Royal Society A-Mathematical Physical and Engineering Sciences* **2013,** *372*, 20130384.
62. Kästner, J., Umbrella Sampling. *WIREs Computational Molecular Science* **2011,** *1*, 932-942.
63. Gao, J.; Truhlar, D. G., Quantum mechanical methods for enzyme kinetics. *Annual Review of Physical Chemistry* **2002,** *53*, 467-505.
64. Sato, S., A New Method of Drawing the Potential Energy Surface. *Bulletin of the Chemical Society of Japan* **1955,** *28* (7), 450-453.
65. Sato, S., Potential Energy Surface of the System of Three Atoms. *Journal of Chemical Physics* **1955,** *23*, 2465-2466.
66. Glowacki, D. R.; Orr-Ewing, A. J.; Harvey, J. N., Product energy deposition of CN + alkane H abstraction reactions in gas and solution phases. *Journal of Chemical Physics* **2011,** *134*, 214508.
67. Glowacki, D. R.; Orr-Ewing, A. J.; Harvey, J. N., Non-equilibrium reaction and relaxation dynamics in a strongly interacting explicit solvent: F + CD_3CN treated with a parallel multi-state EVB model. *Journal of Chemical Physics* **2015,** *143* (4), 044120.
68. Purvis, G. D.; Bartlett, R. J., A full coupled-cluster singles and doubles model: The inclusion of disconnected triples. *Journal of Chemical Physics* **1982,** *76* (4), 1910-1918.
69. Scuseria, G. E.; Janssen, C. L.; Schaefer, H. F., An efficient reformulation of the closed-shell coupled cluster single and double excitation (CCSD) equations. *Journal of Chemical Physics* **1988,** *89* (12), 7382-7387.
70. Scuseria, G. E.; Schaefer, H. F., Is coupled cluster singles and doubles (CCSD) more computationally intensive than quadratic configuration interaction (QCISD)? *Journal of Chemical Physics* **1989,** *90* (7), 3700-3703.
71. Dunning, T. H., Jr., Gaussian basis sets for use in correlated molecular calculations. I. The atoms boron through neon and hydrogen. *Journal of Chemical Physics* **1989,** *90* (2), 1007-1023.
72. Kendall, R. A.; Dunning, T. H., Jr.; Harrison, R. J., Electron affinities of the first-row atoms revisited. Systematic basis sets and wave functions. *Journal of Chemical Physics* **1992,** *96* (9), 6796-6806.

73. Frisch, M. J.; Trucks, G. W.; Schlegel, H. B.; Scuseria, G. E.; Robb, M. A.; Cheeseman, J. R.; Scalmani, G.; Barone, V.; Mennucci, B.; Petersson, G. A., Gaussian 09, Gaussian, Inc.: Wallingford, CT, USA, 2009.
74. Miyoshi, A. GPOP software, rev. 2013.07.15m7. (accessed April 10, 2019).
75. Brooks, B. R.; Bruccoleri, R. E.; Olafson, B. D.; States, D. J.; Swaminathan, S.; Karplus, M., CHARMM - a program for macromolecular energy, minimization, and dynamics calculations. *Journal of Computational Chemistry* **1983,** *4* (2), 187-217.
76. Brooks, B. R.; Brooks, C. L.; Mackerell, A. D.; Nilsson, L.; Petrella, R. J.; Roux, B.; Won, Y.; Archontis, G.; Bartels, C.; Boresch, S., et al., CHARMM: The biomolecular simulation program. *Journal of Computational Chemistry* **2009,** *30* (10), 1545-1614.
77. Kuchitsu, K., *Structure of Free Polyatomic Molecules - Basic Data*. Springer: Berlin, 1998.
78. Perez-Blanco, M. E.; Maginn, E. J., Molecular Dynamics Simulations of CO_2 at an Ionic Liquid Interface: Adsorption, Ordering, and Interfacial Crossing. *Journal of Physical Chemistry B* **2010,** *114*, 11827-11837.
79. Potoff, J. J.; Siepmann, J. I., Vapor-liquid equilibria of mixtures containing alkanes, carbon dioxide, and nitrogen. *Aiche Journal* **2001,** *47* (7), 1676-1682.
80. Aimoli, C. G.; Maginn, E. J.; Abreu, C. R. A., Force field comparison and thermodynamic property calculation of supercritical CO2 and CH4 using molecular dynamics simulations. *Fluid Phase Equilibria* **2014,** *368*, 80-90.
81. Nose, S., A unified formulation of the constant temperature molecular dynamics methods. *Journal of Chemical Physics* **1984,** *81* (1), 511-519.
82. Hoover, W. G., Canonical dynamics: Equilibrium phase-space distributions. *Physical Review A* **1985,** *31* (3), 1695-1697.
83. Darden, T.; York, D.; Pedersen, L., Particle mesh Ewald: An N log(N) method for Ewald sums in large systems. *Journal of Chemical Physics* **1993,** *98* (12), 10089-10092.
84. Essmann, U.; Perera, L.; Berkowitz, M. L.; Darden, T.; Lee, H.; Pedersen, L. G., A smooth particle mesh Ewald method. *The Journal of Chemical Physics* **1995,** *103* (19), 8577-8593.
85. Fernández-Ramos, A.; Miller, J. A.; Klippenstein, S. J.; Truhlar, D. G., Modeling the Kinetics of Bimolecular Reactions. *Chemical Reviews* **2006,** *106*, 4518-4584.

TOC Graphic